Atmos. Meas. Tech. Discuss., 4, 2127–2159, 2011
www.atmos-meas-tech-discuss.net/4/2127/2011/
doi:10.5194/amtd-4-2127-2011

Atmospheric Measurement Techniques Discussions

An assessment of differences in lower stratospheric temperature records from (A)MSU, radiosondes, and GPS radio occultation

F. Ladstädter[1], A. K. Steiner[1], U. Foelsche[1], L. Haimberger[2], C. Tavolato[2], and G. Kirchengast[1]

[1]Wegener Center for Climate and Global Change (WEGC) and Institute for Geophysics, Astrophysics, and Meteorology/Inst. of Physics (IGAM/IP), University of Graz, Austria
[2]Department of Meteorology and Geophysics, University of Vienna, Austria

Received: 1 March 2011 – Accepted: 3 April 2011 – Published: 7 April 2011

Correspondence to: F. Ladstädter (florian.ladstaedter@uni-graz.at)

Published by Copernicus Publications on behalf of the European Geosciences Union.

Abstract

Uncertainties for upper-air trend patterns are still substantial. Observations from the radio occultation (RO) technique offer new opportunities to assess the existing observational records there. Long-term time series are available from radiosondes and from the (Advanced) Microwave Sounding Unit (A)MSU. None of them were originally intended to deliver data for climate applications. Demanding intercalibration and homogenization procedures are required to account for changes in instrumentation and observation techniques. In this comparative study three (A)MSU anomaly time series and two homogenized radiosonde records are compared to RO data from the CHAMP, SAC-C, GRACE-A and F3C missions for September 2001 to December 2009. Differences of monthly anomalies are examined to assess the differences in the datasets due to structural uncertainties. The difference of anomalies of the (A)MSU datasets relative to RO shows a statistically significant trend of about (-0.2 ± 0.05) K at all latitudes. This signals a divergence of the two datasets over time. The radiosonde network has known deficiencies in its global coverage, with sparse representation of most of the Southern Hemisphere, the tropics and the oceans. In this study the error that results from sparse sampling is estimated and accounted for by subtracting it from radiosonde and RO datasets. Surprisingly the sampling error correction is also important in the Northern Hemisphere (NH), where the radiosonde network is dense over the continents but does not capture large atmospheric variations in NH winter. Considering the sampling error, the consistency of radiosonde and RO anomalies is improving substantially; there is no significant trend in the anomaly differences at global scale and in the NH. Regarding (A)MSU, its poor vertical resolution poses another problem by missing important features of the vertical atmospheric structure. This demonstrates the advantage of homogeneously distributed measurements with high vertical resolution.

AMTD
4, 2127–2159, 2011

1 Introduction

The upper troposphere-lower stratosphere (UTLS) region is known to react sensitively to climate change (Baldwin et al., 2007). High-quality observations are crucial to assess the anthropogenic influence on the climate system in the UTLS. It is well known that the temperature trend patterns in the troposphere and stratosphere can provide valuable information on the mechanisms of climate change (Karl et al., 2006; Solomon et al., 2007; Thompson and Solomon, 2005). Until now observational data exist primarily from radiosondes (since 1958) and from the (Advanced) Microwave Sounding Unit (A)MSU instrument flying on US National Oceanic and Atmospheric Administration (NOAA) polar orbiting satellites (since 1979). However, none of these existing long-term measurement systems for the upper-air were originally intended to be used for climate monitoring purposes. While surface temperature trends are in accordance amongst different groups (Solomon et al., 2007), the uncertainties regarding trend values for the upper-air are still substantial (Randel et al., 2009; Randall and Herman, 2008; Titchner et al., 2009). The main reasons for these uncertainties derive from demanding intercalibration and homogenization procedures. These *structural uncertainties* have been results of changing instrumentation and observation practice over the decades (Karl et al., 2006; Thorne et al., 2005). This is true for both main sources of upper-air temperature data. The radiosonde time series has specifically experienced numerous changes in their stations, types of sensors, and changes in data processing systems. Using advanced homogenization techniques, these artificial data discontinuities are reduced (Haimberger, 2007; Haimberger et al., 2008). The sparse spatial sampling is causing further uncertainties in the global radiosonde stations' network (Free and Seidel, 2005). Unlike radiosondes, (A)MSU data provide very good global coverage. The instrumentation biases introduced in the chain of NOAA satellites (most recent being NOAA-19) still need to be accounted for. Further errors affecting (A)MSU data include shifts in the diurnal sampling, orbit variations and calibration changes (Karl et al., 2006). Many of these issues are addressed by calibrated datasets produced by different groups (Christy et al., 2007; Mears and Wentz, 2009; Zou et al., 2009).

AMTD
4, 2127–2159, 2011

There have been significant efforts in the past to create reliable climate records despite these obstacles (Mears and Wentz, 2009; Christy et al., 2003; Haimberger et al., 2008; Zou and Wang, 2010). It has been argued that the uncertainties in upper-air temperature trends are inevitable due to structural uncertainties involved in the methodology (Thorne et al., 2005). Increasing the number of independent datasets decreases the structural uncertainty (Seidel et al., 2004). The need for new upper-air measurement systems has already been stated by the implementation plan for the Global Observing System for Climate (GCOS, 2010). One already existing relatively new system is GPS radio occultation (RO) that can be considered as of potential benchmark quality (Steiner et al., 2009b). RO uses Global Positioning System (GPS) radio signals in limb sounding geometry to deliver observations in the UTLS region with high accuracy, global coverage, and high vertical resolution (Melbourne et al., 1994; Kursinski et al., 1997; Steiner et al., 2001; Hajj et al., 2002). Additionally it is self-calibrating, thus avoiding error-prone intercalibration procedures. These properties make the technique well qualified to be used for climate applications, as has been shown in a considerable number of publications (e.g., Scherllin-Pirscher et al., 2011b; Steiner et al., 2009b; Foelsche et al., 2009; Ho et al., 2009b; Leroy et al., 2006). Therefore RO can be considered a good choice to assess the adequacy of the observational data mentioned above for climate applications. This has been done in several previous studies for (A)MSU (Schrøder et al., 2003; Ho et al., 2007; Steiner et al., 2007, 2009a). Regarding radiosondes, Kuo et al. (2005), He et al. (2009), and Sun et al. (2010) concluded that RO soundings are of sufficient quality to differentiate between different types of radiosondes. Steiner et al. (2007, 2009a), and Ho et al. (2007) found significant differences between RO and (A)MSU climatologies. Ho et al. (2009a) suggested to use RO data for calibration of (A)MSU temperatures.

This study advances previous work (Steiner et al., 2007), using the most recent datasets for RO, (A)MSU and radiosondes, and substantially longer records. It furthermore improves on previous work by analysing error characteristics of RO and radiosondes resulting from sparse spatial and temporal sampling. The data used in this study

AMTD
4, 2127–2159, 2011

are briefly introduced in Sect. 2, the method of comparison and assessing sampling error characteristics is described in Sect. 3, the results are discussed in Sect. 4, followed by a summary of the results and conclusions of this comparative study.

2 Data

The comparison time range is limited by the availability of continuous RO data. The CHAMP satellite (Wickert et al., 2001) delivered data from September 2001 to September 2008. Data from the FORMOSAT-3/COSMIC (F3C) mission (Anthes et al., 2008) are used starting from August 2006 until December 2009. Available data from SAC-C (2001, 2002) (Hajj et al., 2004) and GRACE-A (2007 to 2009) (Beyerle et al., 2005) are also used. The study time frame is therefore September 2001 to December 2009 (Fig. 1).

2.1 GPS radio occultation

We use CHAMP, SAC-C, GRACE-A, and F3C profiles from September 2001 to December 2009 as processed by the Wegener Center for Climate and Global Change (WEGC). We applied the current processing scheme OPSv5.4 (Occultation Processing System, version 5.4) to excess phase profiles and precise orbit information provided by the University Corporation for Atmospheric Research (UCAR) (Pirscher, 2010). The data of the various instruments can be combined to a consistent single climate record as long as the processing chain is the same for all sources (Pirscher, 2010; Foelsche et al., 2011). Only high-quality profiles are used in a height range of 0.1 km to 35 km. These profiles can be downloaded from the global climate monitoring website[1]. The number of profiles ranges from about 100 to 150 per day (single-satellite) up to about 2000 per day (multi-satellite); see the representative example months in Fig. 2. The observations are distributed almost uniformly in both cases.

[1] www.wegcenter.at/globclim

AMTD
4, 2127–2159, 2011

2.2 (Advanced) Microwave Sounding Unit

The (Advanced) Microwave Sounding Unit ([A]MSU) instruments provide satellite-based nadir measurements of layer-average brightness temperatures. The instruments fly on board of the NOAA series of polar orbiting satellites. We use calibrated post-processed data from three different groups, all of them provided at $2.5^\circ \times 2.5^\circ$ horizontal resolution. The AMSU instruments are in orbit since 1998, while the last NOAA satellite with a MSU instrument aboard was decommissioned in 2004. Therefore, during this overlap time contained in the study time frame, the (A)MSU datasets include data from both instrument types.

The bulk temperature of the lower stratosphere region (TLS) corresponds to MSU channel 4 and AMSU channel 9, respectively. These two channels closely match each other purposely, to ensure continuation of the temperature time series. The layer between 150 hPa and 30 hPa (≈13 km to 25 km) contributes most to the TLS layer mean temperature, peaking at around 90 hPa (≈18 km) (Christy et al., 2003). The poor vertical resolution results in considerable influence of the troposphere to the TLS in the tropics.

TLS brightness temperatures were retrieved from the University of Alabama at Huntsville (UAH) (Christy et al., 2003) in version UAHv5.3[2]; from Remote Sensing Systems (RSS) (Mears and Wentz, 2009) in version RSSv3.2[3]; and from the National Environmental Satellite, Data and Information Service (NESDIS) Center for Satellite Applications and Research (STAR) (Zou et al., 2009) in version STARv2.0[4].

[2] http://vortex.nsstc.uah.edu/data/msu/

[3] http://www.remss.com/msu/msu_browse.html

[4] ftp://ftp.orbit.nesdis.noaa.gov/pub/smcd/emb/mscat/data/v2.0/

AMTD
4, 2127–2159, 2011

2.3 Radiosondes

For this comparison, we use the latest homogenized radiosonde datasets: the Radiosonde Observation using Reanalysis (RAOBCORE) dataset (Haimberger, 2007) in version RAOBCOREv1.4 and the Radiosonde Innovation Composite Homogenization (RICH) dataset (Haimberger et al., 2008). Both use raw radiosonde data from the Integrated Global Radiosonde Archive (IGRA) and the 40-yr European Centre for Medium-Range Weather Forecasts (ECMWF) Re-Analysis (ERA-40) (Uppala et al., 2004) radiosonde archives. More than 1000 stations are used. 00:00 UTC and 12:00 UTC launches are kept separately. Figure 3 shows the global coverage of these archives and indicates the launch times. The homogenization procedure works on daily data, which enables very effective breakpoint detection.

RAOBCORE uses time series of a background dataset (ERA-Interim; Dee et al., 2009) as reference for homogenization. RAOBCORE is therefore, strictly speaking, not independent of satellite data, because ERA-Interim contains (A)MSU information. RICH uses the breakpoints detected by RAOBCORE, but relies only on neighboring stations for the actual homogenization. It is therefore a completely independent dataset (Haimberger et al., 2008).

For both homogenized radiosonde time series, the University of Vienna constructed MSU-equivalent brightness temperatures (TLS) anomalies on a $2.5^\circ \times 2.5^\circ$ horizontal grid[5].

2.4 ECMWF

As reference dataset in the estimation of sampling error characteristics of RO and radiosondes (see method description in Sect. 3), we use analysis fields created by the ECMWF. For each RO profile, OPSv5.4 extracts a collocated profile from the global ECMWF field (Scherllin-Pirscher et al., 2011b). The analysis fields are available for

[5] http://www.univie.ac.at/theoret-met/research/raobcore/

AMTD
4, 2127–2159, 2011

four time layers, 00:00 UTC, 06:00 UTC, 12:00 UTC, and 18:00 UTC. The 00:00 UTC and 12:00 UTC time layers correspond to the radiosonde launch times and are used in 2.5° × 2.5° horizontal resolution as collocated fields to radiosonde data at station locations. The averaged field over all time layers is used as reference for the radiosondes and RO, as described in the next section.

3 Method

The different comparisons in this study are based on TLS layer-average brightness temperatures ("MSU-equivalent"). We compare monthly and zonal means for regularly-spaced 20° bands and for four regions, tropics (20° S to 20° N), extra-tropics (70° S to 30° S and 30° N to 70° N), and quasi-global (70° S to 70° N).

3.1 Setup of comparable data

We use the Radiative Transfer for TOVS (RTTOV) model (Saunders, 2008) to compute layer-average TLS from RO and collocated ECMWF temperature profiles. To match the horizontal and temporal resolutions of the other datasets, we then bin the resulting TLS field into a 2.5° × 2.5° grid (monthly means). Averaging involves weighting by the cosine of the latitude, which accounts for area changes between meridians of different latitudes (Foelsche et al., 2008). This is only a minor effect at this resolution though. We do not distinguish between the various RO missions, all available RO profiles are incorporated into the respective monthly mean. As noted above, this procedure is justified given that the processing chain is the same for all sources (up to negligible differences in raw processing) and that the inter-satellite consistency is thus very high (Foelsche et al., 2011).

The ECMWF analysis field at 2.5° × 2.5° resolution is also processed by RTTOV separately for all four available time layers. As a result, all datasets involved in this comparison are now available at the same monthly-means, 2.5° × 2.5° resolution and

AMTD
4, 2127–2159, 2011

in MSU-equivalent TLS. In Fig. 4 we show representative TLS fields for RO and differences of RO to STAR for two months (Northern Hemisphere (NH) winter and summer). TLS temperatures of RO and STAR show larger deviations at higher latitudes, but are generally in very good agreement, especially on a zonal mean scale as used below.

In the next step, we create latitudinal bands by simply averaging over all bins at each respective latitude. Then we aggregate those to larger bands. Here we apply weighting with the surface area of the bands involved. This approach accounts for the decreasing area of latitude bands of equal width (Foelsche et al., 2011).

3.2 Sampling error estimation

All observational datasets inherently differ from reality because of their finite sampling of the atmosphere. Depending on the sampling density and the variability of the atmosphere, it often is essential to account for this difference. A decent approach to estimate the magnitude of error made by discrete sampling is to compare climatologies to a "true" reference field (Foelsche et al., 2008). In this study, the sampling error estimation for RO and radiosondes is performed consistently. We do not consider sampling error for (A)MSU because we can assume that the error reaches virtually zero due to high horizontal resolution of the dataset.

We use ECMWF analysis fields for all four time layers assuming that they are valid approximations of the "true" global field. The methodology for estimating the sampling error of RO is described in detail elsewhere (Pirscher, 2010; Foelsche et al., 2008). In short, the collocated ECMWF profiles are averaged to latitudinal bands and monthly means as described above. They represent the atmospheric state at the times and locations of RO measurements as seen by the reference field. We then subtract the full reference field, representing the "true" atmospheric state. We define this difference as *sampling error* of RO for the respective month and latitudinal band. We finally subtract the estimated sampling error from RO climatologies. This substantially improves the quality of RO climatologies as has been shown in several studies (Foelsche et al., 2011; Scherllin-Pirscher et al., 2011a). The actual data is thus not used for estimating the sampling error.

AMTD
4, 2127–2159, 2011

In contrast to satellite measurements, the global coverage of radiosondes is not uniform. Most notable, the Southern Hemisphere (SH), the tropics, and the oceans are sparsely represented. In other regions, especially over the NH continents, the coverage is very good. Free and Seidel (2005) stated that the concentration of stations in those regions does not necessarily improve the dataset because it oversamples those continental areas while under-representing the oceans. At most of the stations in the SH, radiosonde launches occur only once a day, see Fig. 3. Using an equivalent approach as for RO we estimate the sampling error for radiosondes. We take the ECMWF analysis fields for 00:00 UTC and 12:00 UTC separately, and sub-sample the $2.5^{\circ} \times 2.5^{\circ}$ fields to bins where we have radiosonde data for the respective time. This results in a temporally and spatially collocated reference field, analogous to the method above described for RO. After averaging to latitudinal bands we subtract the full reference field containing all four time layers to get the sampling error for radiosondes. Finally we subtract the sampling error from the radiosonde data as we did for RO.

3.3 Computation of TLS anomalies and anomaly differences

For RO and (A)MSU data, we calculate monthly TLS anomalies relative to the period 2002 to 2009 to de-seasonalize the data. The radiosonde time series are already provided in anomaly space for the same reference time period. After subtracting the respective sampling error from RO and radiosonde anomalies (as described above), we compute differences of these anomaly time series. Thereby the climatological variability common to both datasets is removed. Then remaining are the differences due to structural uncertainties. We then compute the linear trends in the anomalies and anomaly differences and their statistical significance to assess deviations between the datasets. In particular, a statistically significant trend of the anomaly differences indicates that both datasets involved behave differently in their time evolution.

AMTD
4, 2127–2159, 2011

4 Results

4.1 Sampling error

Only by considering the sampling error for both RO and radiosonde records, a consistent comparison is possible. In Fig. 5 the resulting sampling error for radiosondes and RO is shown for 20° zonal bands from 90° S to 90° N. For RO, the sampling error is generally very small (<0.2 K), except at high latitudes, where it becomes increasingly difficult to capture atmospheric variability (Scherllin-Pirscher et al., 2011a). For radiosondes (cf. Fig. 5, top), the sampling error is rather small (< 0.3 K) between about 50° S to 50° N. For higher latitudes the sampling error becomes large. We attribute this to greater variability of the atmosphere at higher latitudes and to the small number of stations in the SH. The sampling density in the tropics is also small but seems to be sufficient to capture the main features of atmospheric variability there. The patterns in southern and northern high latitudes differ substantially: while in the SH temporal evolution of the sampling error seems to be a rather random effect related to sparse sampling, the pattern in the NH shows a clear relation to the NH winter. Every NH winter the sampling error reaches a maximum. Comparing with Fig. 4 (top left), showing the TLS pattern in January, implies that the radiosonde network misses the large characteristic difference between Pacific ocean and landmasses in winter. This results in a larger sampling error.

Temporal sampling of radiosondes (00:00 UTC and 12:00 UTC) seems to be sufficient to capture the diurnal cycle. This was investigated by using only 00:00 UTC and 12:00 UTC time layers of the reference field for calculating the sampling error, instead of the "full" field of four time layers. Comparing the sampling error based on 00:00 UTC and 12:00 UTC time layers with that based on the "full" field showed very small differences only.

The effect of subtracting the respective sampling error from RO and radiosonde anomalies is shown in Fig. 6 for the large-scale zonal bands defined above. It is especially pronounced in NH and SH extratropics. The distinct influence of the sampling

AMTD
4, 2127–2159, 2011

error correction in NH winter is clearly visible, as well as the all-year random effect in the SH extratropics. Generally, the radiosonde data get significantly closer to the RO time series after removing the sampling error. In the following, the RO and radiosonde datasets are always being used in the corrected form of having their respective sampling errors subtracted. We focus on 70° S to 70° N to avoid sampling problems at polar latitudes.

4.2 TLS anomalies and anomaly differences

The TLS anomalies of all datasets are shown in Fig. 7 at 20° latitudinal resolution for 70° S to 70° N. Overall, the anomaly patterns of the various datasets are consistent. Figure 8 shows TLS anomaly time series for the investigated large-scale zonal bands. The anomalies show good agreement over the whole time range. The anomaly trend values are summarized in Table 1. We observe statistically significant (at 95% significance level) negative TLS trends in the global mean for all (A)MSU datasets. These negative trends mostly stem from the extratropics, in particular from the SH. The trend values of −0.3 K to −1.0 K per decade are in agreement with Randel et al. (2009). In the tropics the trend values are the smallest, and RO, RSS and RAOBCORE even show positive trend values (statistically not significant) for the TLS brightness temperature anomalies there. This probably is a result from the coarse vertical resolution of TLS MSU-equivalents, where TLS derives from integrating over upper troposphere/lower stratosphere parts of the tropics (Randel et al., 2009). As shown by Schmidt et al. (2010), RO detects a strongly positive trend signal in the tropics around the tropical tropopause, most probably strongly influencing the integral TLS. We do not further enter here into a climatological interpretation of the trends (which is difficult because of the short time period involved) but focus below on the structural differences of the datasets.

The differences of radiosonde and (A)MSU anomalies to RO anomalies are shown in Fig. 9 at 20° latitudinal resolution and in Fig. 10 for the large-scale zonal regions. The anomaly difference trend values are summarized in Table 2. RAOBCORE and

AMTD
4, 2127–2159, 2011

RICH show nearly negligible trends in their difference to RO, (0.05 ± 0.06) K and (-0.04 ± 0.07) K globally, which indicates that they do not diverge in time relative to RO. A notable exception of this can be observed in the tropics, which is likely related to sparse radiosonde station number in this region. The TLS anomaly difference trend of radiosondes relative to RO is larger for the RICH dataset in the tropics and SH. RICH adjustments tend to be noisier than RAOBCORE especially in the tropics and SH because the distance between neighboring stations becomes large, whereas RAOBCORE adjustments need no interpolation. They are just derived from ERA-Interim background fields. The above mentioned problem of the radiosonde network to correctly capture NH winter atmospheric variations is visible in the NH and quasi-global latitudinal bands. These differences are much more pronounced if the radiosonde datasets are not corrected for their sampling error (not shown; cf. Fig. 6).

The TLS anomaly difference trend of (A)MSU relative to RO is about (-0.2 ± 0.05) K, consistent throughout all latitude ranges. Difference trends of RSS to RO are generally slightly smaller than for UAH and STAR (with the exception of the SH extratropics).

These results are summarized in Fig. 11, and include the respective difference of the radiosonde datasets to a representative (A)MSU dataset (STAR) and the difference of RAOBCORE to RICH, all with their 95% confidence interval.

5 Summary and conclusions

This study focused on comparing (A)MSU data and radiosonde data to radio occultation data, which are well qualified as reference dataset for climate applications. We included RO data from CHAMP, SAC-C, GRACE-A, and F3C satellites for the time period September 2001 to December 2009. All RO profiles were transformed to MSU-equivalent layer-average brightness temperatures (TLS) using a radiative transfer model (RTTOV). Using inter-satellite consistency, the RO data were combined to form a single TLS RO climatology dataset. This dataset was compared to (A)MSU datasets (UAH, RSS, STAR) and recent homogenized radiosonde datasets (RAOBCORE, RICH).

AMTD
4, 2127–2159, 2011

We estimated the spatiotemporal sampling error of radiosonde and RO data. Comparing the RO reference climatology with radiosondes, we showed the importance of taking into account these error characteristics also for radiosondes. The consistency of radiosondes and RO was improved substantially by subtracting their respective sampling errors. We thus compared radiosonde and RO datasets in corrected form, i.e., with their sampling errors subtracted. The resulting anomaly time series for TLS showed good agreement of radiosonde data with RO.

Rather surprisingly, we found that it is also important to take into account the sampling error for radiosondes in the Northern Hemisphere (NH) extratropics where radiosonde station coverage is generally very good. We conclude that this results from the radiosonde network missing the atmospheric variability over the oceans, particularly in NH winter. The advantage of homogeneously distributed measurements is thus clearly visible. In the tropics the deviations of radiosonde TLS from RO TLS are relatively small. This implies that despite the small number of stations in this region the sampling of radiosondes seems to be sufficient to largely capture the relatively homogeneous atmosphere in the tropics. RAOBCORE showed less difference compared to RO than RICH in the tropics and SH though, because RAOBCORE adjustments do not need interpolation involving neighboring stations. Generally radiosonde data showed larger errors in SH than elsewhere because the station coverage is very sparse there. Trends in TLS anomaly differences of radiosondes compared to RO were found to be insignificant in the global mean, (0.05 ± 0.06) K for RAOBCORE and (-0.04 ± 0.07) K for RICH.

(A)MSU data do not need sampling error correction because they provide very dense horizontal sampling. We found statistically significant trend values of about (-0.2 ± 0.05) K for the anomaly differences relative to RO in all large-scale zonal regions. This latitudinally consistent result somewhat deviates from the results of Steiner et al. (2007), who showed significant difference trends mainly in the tropics for the time period 2001 to 2006. We suppose that the time range in Steiner et al. (2007) was still too short to detect significant trends in all latitude ranges. The trend values for

AMTD
4, 2127–2159, 2011

the anomaly differences were found slightly smaller for RSS than for UAH and STAR, except in the SH extratropics.

In the tropics the trend of anomaly differences relative to RO was statistically significant for all datasets involved. This indicates that a better vertical resolution (than provided by layer-average TLS of the (A)MSU instrument) is of advantage. It also points to the fact that the remaining differences are likely easiest to explain in the tropics (which we will analyze in a future study). Given that radiosonde and RO trends statistically agree in regions well covered by radiosonde data (NH extratropics and quasi-global domains) indicates that the detected differences mainly stem from the (A)MSU data.

Acknowledgements. We are grateful to UCAR/CDAAC (USA) and WEGC (A) GPS RO operational team members for provision of RO data, at WEGC especially to J. Fritzer and B. Scherllin-Pirscher for their contributions to OPS system development and operations. UAH, RSS and NESDIS/STAR (all USA) are acknowledged for providing (A)MSU records. We thank B. C. Lackner for fruitful discussions. Furthermore we thank ECMWF (UK) for access to their atmospheric analysis data. This work was funded by the Austrian Science Fund (FWF; BENCHCLIM project P22293-N21, TRENDEVAL project P21642-N21, C. Tavolato and L. Haimberger supported by project P21772-N10). WEGC OPS development was co-funded by ESA/ESTEC Noordwijk, ESA/ESRIN Frascati, and FFG/ALR Austria.

References

Anthes, R. A., Ector, D., Hunt, D. C., Kuo, Y.-H., Rocken, C., Schreiner, W. S., Sokolovskiy, S. V., Syndergaard, S., Wee, T.-K., Zeng, Z., Bernhardt, P. A., Dymond, K. F., Chen, Y., Liu, H., Manning, K., Randel, W. J., Trenberth, K. E., Cucurull, L., Healy, S. B., Ho, S.-P., McCormick, C., Meehan, T. K., Thompson, D. C., and Yen, N. L.: The COSMIC/FORMOSAT-3 Mission: Early Results, B. Am. Meteorol. Soc., 89, 313–333, doi:10.1175/BAMS-89-3-313, 2008. 2131

Baldwin, M. P., Dameris, M., and Shepherd, T. G.: How Will the Stratosphere Affect Climate Change?, Science, 316, 1576–1577, doi:10.1126/science.1144303, 2007. 2129

Beyerle, G., Schmidt, T., Michalak, G., Heise, S., Wickert, J., and Reigber, C.: GPS radio occul-

AMTD

4, 2127–2159, 2011

tation with GRACE: Atmospheric profiling utilizing the zero difference technique, Geophys. Res. Lett., 32, L13806, doi:10.1029/2005GL023109, 2005. 2131
Christy, J. R., Spencer, R. W., Norris, W. B., Braswell, W. D., and Parker, D. E.: Error Estimates of Version 5.0 of MSU–AMSU Bulk Atmospheric Temperatures, J. Atmos. Ocean. Tech., 20, 613–629, doi:10.1175/1520-0426(2003)20<613:EEOVOM>2.0.CO;2, 2003. 2130, 2132
Christy, J. R., Norris, W. B., Spencer, R. W., and Hnilo, J. J.: Tropospheric temperature change since 1979 from tropical radiosonde and satellite measurements, J. Geophys. Res., 112, D06102, doi:10.1029/2005JD006881, 2007. 2129
Dee, D., Berrisford, P., Poli, P., and Fuentes, M.: ERA-Interim for climate monitoring, ECMWF Newsletter No. 119–Spring 2009, 2009. 2133
Foelsche, U., Borsche, M., Steiner, A., Gobiet, A., Pirscher, B., Kirchengast, G., Wickert, J., and Schmidt, T.: Observing upper troposphere–lower stratosphere climate with radio occultation data from the CHAMP satellite, Clim. Dynam., 31, 49–65, doi:10.1007/s00382-007-0337-7, 2008. 2134, 2135
Foelsche, U., Pirscher, B., Borsche, M., Kirchengast, G., and Wickert, J.: Assessing the climate monitoring utility of radio occultation data: From CHAMP to FORMOSAT-3/COSMIC, Terr. Atmos. Ocean. Sci., 20, 155–170, doi:10.3319/TAO.2008.01.14.01(F3C), 2009. 2130
Foelsche, U., Scherllin-Pirscher, B., Ladstädter, F., Steiner, A. K., and Kirchengast, G.: Refractivity and temperature climate records from multiple radio occultation satellites consistent within 0.05%, Atmos. Meas. Tech. Discuss., 4, 1593–1615, doi:10.5194/amtd-4-1593-2011, 2011. 2131, 2134, 2135
Free, M. and Seidel, D. J.: Causes of differing temperature trends in radiosonde upper air data sets, J. Geophys. Res., 110, D07101, doi:10.1029/2004JD005481, 2005. 2129, 2136
GCOS: Implementation plan for the Global Observing System for Climate in support of the UNFCCC, (2010 Update), WMO-TD/No. 1523 GCOS-138 (GOOS-184, GTOS-76), WMO, 2010. 2130
Haimberger, L.: Homogenization of Radiosonde Temperature Time Series Using Innovation Statistics, J. Climate, 20, 1377–1403, doi:10.1175/JCLI4050.1, 2007. 2129, 2133
Haimberger, L., Tavolato, C., and Sperka, S.: Toward Elimination of the Warm Bias in Historic Radiosonde TemperatureRecords—Some New Results from a Comprehensive Intercomparison of Upper-Air Data, J. Climate, 21, 4587–4606, doi:10.1175/2008JCLI1929.1, 2008. 2129, 2130, 2133
Hajj, G. A., Kursinski, E. R., Romans, L. J., Bertiger, W. I., and Leroy, S. S.: A technical

AMTD
4, 2127–2159, 2011

description of atmospheric sounding by GPS occultation, J. Atmos. Sol-Terr. Phy., 64, 451–469, doi:10.1016/S1364-6826(01)00114-6, 2002. 2130

Hajj, G. A., Ao, C. O., Iijima, B. A., Kuang, D., Kursinski, E. R., Mannucci, A. J., Meehan, T. K., Romans, L. J., de la Torre Juarez, M., and Yunck, T. P.: CHAMP and SAC-C atmospheric occultation results and intercomparisons, J. Geophys. Res., 109, D06109, doi:10.1029/2003JD003909, 2004. 2131

He, W., Ho, S.-p., Chen, H., Zhou, X., Hunt, D., and Kuo, Y.-H.: Assessment of radiosonde temperature measurements in the upper troposphere and lower stratosphere using COSMIC radio occultation data, Geophys. Res. Lett., 36, L17807, doi:10.1029/2009GL038712, 2009. 2130

Ho, S.-P., Kuo, Y.-H., Zeng, Z., and Peterson, T.: A comparison of lower stratosphere temperature from microwave measurements with CHAMP GPS RO data, Geophys. Res. Lett., 34, L15701, doi:10.1029/2007GL030202, 2007. 2130

Ho, S. P., Goldberg, M., Kuo, Y. H., Zou, C. Z., and Schreiner, W.: Calibration of temperature in the lower stratosphere from microwave measurements using COSMIC Radio Occultation data: preliminary results, Terr. Atmos. Ocean. Sci., 20, 87–100, doi:10.3319/TAO.2007.12.06.01(F3C), 2009a. 2130

Ho, S.-P., Kirchengast, G., Leroy, S., Wickert, J., Mannucci, T., Steiner, A., Hunt, D., Schreiner, W., Sokolovskiy, S., Ao, C., Borsche, M., von Engeln, A., Foelsche, U., Heise, S., Iijima, B., Kuo, Y.-H., Kursinski, E., Lackner, B., Pirscher, B., Ringer, M., Rocken, C., , and Schmidt, T.: Estimating the Uncertainty of using GPS Radio Occultation Data for Climate Monitoring: Intercomparison of CHAMP Refractivity Climate Records from 2002 to 2006 from Different Data Centers, J. Geophys. Res., 114, D23107, doi:10.1029/2009JD011969, 2009b. 2130

Karl, T. R., Hassol, S. J., Miller, C. D., and Murray, W. L. (Eds.): Temperature Trends in the Lower Atmosphere: Steps for Understanding and Reconciling Differences, U.S. Climate Change Science Program/Subcommittee on Global Change Research, 2006. 2129

Kuo, Y.-H., Schreiner, W. S., Wang, J., Rossiter, D. L., and Zhang, Y.: Comparison of GPS radio occultation soundings with radiosondes, Geophys. Res. Lett., 32, L05817, doi:10.1029/2004GL021443, 2005. 2130

Kursinski, E. R., Hajj, G. A., Schofield, J. T., Linfield, R. P., and Hardy, K. R.: Observing Earth's atmosphere with radio occultation measurements using the Global Positioning System, J. Geophys. Res., 102, 23429–23465, 1997. 2130

Leroy, S., Dykema, J., and Anderson, J.: Climate Benchmarking Using GNSS Occultation, in:

AMTD
4, 2127–2159, 2011

Atmosphere and Climate: Studies by Occultation Methods, edited by Foelsche, U., Kirchengast, G., and Steiner, A., 287–301, Springer Berlin Heidelberg, doi:10.1007/3-540-34121-8_24, 2006. 2130

Mears, C. A. and Wentz, F. J.: Construction of the RSS V3.2 Lower-Tropospheric Temperature Dataset from the MSU and AMSU Microwave Sounders, J. Atmos. Ocean. Tech., 26, 1493–1509, doi:10.1175/2009JTECHA1237.1, 2009. 2129, 2130, 2132

Melbourne, W. G., Davis, E. S., Duncan, C. B., Hajj, G. A., Hardy, K. R., Kursinski, E. R., Meehan, T. K., Young, L. E., and Yunck, T. P.: The application of spaceborne GPS to atmospheric limb sounding and global change monitoring, JPL Publication, 94–18, 147, 1994. 2130

Pirscher, B.: Multi-Satellite Climatologies of Fundamental Atmospheric Variables From Radio Occultation and Their Validation, Ph.D. thesis, Wegener Center for Climate and Global Change and Institute for Geophysics, Astrophysics, and Meteorology, University of Graz, 2010. 2131, 2135

Randall, R. M. and Herman, B. M.: Using limited time period trends as a means to determine attribution of discrepancies in microwave sounding unit-derived tropospheric temperature time series, J. Geophys. Res., 113, D05105, doi:10.1029/2007JD008864, 2008. 2129

Randel, W. J., Shine, K. P., Austin, J., Barnett, J., Claud, C., Gillett, N. P., Keckhut, P., Langematz, U., Lin, R., Long, C., Mears, C., Miller, A., Nash, J., Seidel, D. J., Thompson, D. W. J., Wu, F., and Yoden, S.: An update of observed stratospheric temperature trends, J. Geophys. Res., 114, D02107, doi:10.1029/2008JD010421, 2009. 2129, 2138

Saunders, R.: RTTOV-9 Science and Validation Report, NWP SAF NWPSAF-MO-TV-020, EUMETSAT, 2008. 2134

Scherllin-Pirscher, B., Kirchengast, G., Steiner, A., Kuo, Y.-H., and Foelsche, U.: Quantifying uncertainty in climatological fields from GPS radio occultation: An empirical-analytical error model, Atmos. Meas. Tech. Discuss., submitted, 2011a. 2135, 2137

Scherllin-Pirscher, B., Steiner, A., Kirchengast, G., Kuo, Y.-H., and Foelsche, U.: Empirical analysis and modeling of errors of atmospheric profiles from GPS radio occultation, Atmos. Meas. Tech. Discuss., submitted, 2011b. 2130, 2133

Schmidt, T., Wickert, J., and Haser, A.: Variability of the upper troposphere and lower stratosphere observed with GPS radio occultation bending angles and temperatures, J. Adv. Space Res., 46, 150–161, doi:10.1016/j.asr.2010.01.021, 2010. 2138

Schrøder, T., Leroy, S., Stendel, M., and Kaas, E.: Validating the microwave sounding unit stratospheric record using GPS occultation, Geophys. Res. Lett., 30, 1734,

AMTD
4, 2127–2159, 2011

doi:10.1029/2003GL017588, 2003. 2130
Seidel, D. J., Angell, J. K., Christy, J., Free, M., Klein, S. A., Lanzante, J. R., Mears, C., Parker, D., Schabel, M., Spencer, R., Sterin, A., Thorne, P., and Wentz, F.: Uncertainty in Signals of Large-Scale Climate Variations in Radiosonde and Satellite Upper-Air Temperature Datasets, J. Climate, 17, 2225–2240, doi:10.1175/1520-0442(2004)017<2225:UISOLC>2.0.CO;2, 2004. 2130
Solomon, S., Qin, D., Manning, M., Chen, Z., Marquis, M., Averyt, K., Tignor, M., and Miller, H., eds.: IPCC, 2007: Climate Change 2007: The Physical Science Basis. Contribution of Working Group I to the Fourth Assessment Report of the Intergovernmental Panel on Climate Change, Cambridge University Press, Cambridge, United Kingdom and New York, NY, USA, 2007. 2129
Steiner, A., Kirchengast, G., Borsche, M., Foelsche, U., and Schoengassner, T.: A multi-year comparison of lower stratospheric temperatures from CHAMP radio occultation data with MSU/AMSU records, J. Geophys. Res., 112, D22110, doi:10.1029/2006JD008283, 2007. 2130, 2140
Steiner, A., Kirchengast, G., Borsche, M., and Foelsche, U.: Lower Stratospheric Temperatures from CHAMP RO Compared to MSU/AMSU Records: An Analysis of Error Sources, in: New Horizons in Occultation Research: Studies in Atmosphere and Climate, edited by Steiner, A., Pirscher, B., Foelsche, U., and Kirchengast, G., Springer, Berlin Heidelberg, 2009a. 2130
Steiner, A., Kirchengast, G., Lackner, B., Pirscher, B., Borsche, M., and Foelsche, U.: Atmospheric Temperature Change Detection with GPS Radio Occultation 1995 to 2008, Geophys. Res. Lett., 36, L18702, doi:10.1029/2009GL039777, 2009b. 2130
Steiner, A. K., Kirchengast, K., Foelsche, U., Kornblueh, L., Manzini, E., and Bengtsson, L.: GNSS occultation sounding for climate monitoring, Phys. Chem. Earth, 26, 113–124, doi:10.1016/S1464-1895(01)00034-5, 2001. 2130
Sun, B., Reale, A., Seidel, D. J., and Hunt, D. C.: Comparing radiosonde and COSMIC atmospheric profile data to quantify differences among radiosonde types and the effects of imperfect collocation on comparison statistics, J. Geophys. Res., 115, D23104, doi:10.1029/2010JD014457, 2010. 2130
Thompson, D. W. J. and Solomon, S.: Recent Stratospheric Climate Trends as Evidenced in Radiosonde Data: Global Structure and Tropospheric Linkages, J. Climate, 18, 4785–4795, doi:10.1175/JCLI3585.1, 2005. 2129
Thorne, P. W., Parker, D. E., Christy, J. R., and Mears, C. A.: Uncertainties in Climate Trends:

AMTD
4, 2127–2159, 2011

Lessons from Upper-Air Temperature Records, B. Am. Meteorol. Soc., 86, 1437–1442, doi:10.1175/BAMS-86-10-1437, 2005. 2129, 2130

Titchner, H. A., Thorne, P. W., McCarthy, M. P., Tett, S. F. B., Haimberger, L., and Parker, D. E.: Critically Reassessing Tropospheric Temperature Trends from Radiosondes Using Realistic Validation Experiments, J. Climate, 22, 465–485, doi:10.1175/2008JCLI2419.1, 2009. 2129

Uppala, S., Kållberg, P., Hernandez, A., Saarinen, S., Fiorino, M., Li, X., Onogi, K., Sokka, N., Andrae, U., and Da Costa Bechtold, V.: ERA-40: ECMWF 45-year reanalysis of the global atmosphere and surface conditions 1957–2002, ECMWF Newsletter No. 101–Summer/Autumn 2004, 2004. 2133

Wickert, J., Reigber, C., Beyerle, G., König, R., Marquardt, C., Schmidt, T., Grunwaldt, L., Galas, R., Meehan, T. K., Melbourne, W. G., and Hocke, K.: Atmosphere sounding by GPS radio occultation: First results from CHAMP, Geophys. Res. Lett., 28, 3263–3266, doi:10.1029/2001GL013117, 2001. 2131

Zou, C.-Z. and Wang, W.: Stability of the MSU-Derived Atmospheric Temperature Trend, J. Atmos. Ocean. Tech., 27, 1960–1971, doi:10.1175/2009JTECHA1333.1, 2010. 2130

Zou, C.-Z., Gao, M., and Goldberg, M. D.: Error Structure and Atmospheric Temperature Trends in Observations from the Microwave Sounding Unit, J. Climate, 22, 1661–1681, doi:10.1175/2008JCLI2233.1, 2009. 2129, 2132

AMTD
4, 2127–2159, 2011

Table 1. Trends of anomalies for the period of September 2001 to December 2009. The ± value defines the 95% confidence intervals for the trends. Trend values which are significantly different from 0 at the 90% and 95% level are marked by a single and double asterisk, respectively.

Dataset	Trend (K/8 yr)	$StdDev_{Residuals}$ (K)
70° S to 70° N		
RO	−0.066 ± 0.116	0.18
RAOBCORE	−0.013 ± 0.111	0.17
RICH	−0.104 ± 0.112*	0.17
UAH	−0.259 ± 0.112**	0.17
RSS	−0.247 ± 0.115**	0.18
STAR	−0.268 ± 0.110**	0.17
20° S to 20° N		
RO	+0.183 ± 0.324	0.50
RAOBCORE	+0.084 ± 0.339	0.52
RICH	−0.054 ± 0.335	0.51
UAH	−0.012 ± 0.326	0.50
RSS	+0.014 ± 0.342	0.52
STAR	−0.026 ± 0.322	0.49
30° N to 70° N		
RO	−0.055 ± 0.308	0.47
RAOBCORE	−0.001 ± 0.303	0.47
RICH	−0.087 ± 0.303	0.46
UAH	−0.264 ± 0.308*	0.47
RSS	−0.235 ± 0.314	0.48
STAR	−0.269 ± 0.300*	0.46
70° S to 30° S		
RO	−0.587 ± 0.416**	0.64
RAOBCORE	−0.687 ± 0.445**	0.68
RICH	−0.736 ± 0.438**	0.67
UAH	−0.794 ± 0.434**	0.67
RSS	−0.818 ± 0.438**	0.67
STAR	−0.789 ± 0.428**	0.66

AMTD
4, 2127–2159, 2011

Table 2. Trends of anomaly differences for the period of September 2001 to December 2009. The ± value defines the 95% confidence intervals for the trends. Trend values which are significantly different from 0 at the 90% and 95% level are marked by a single and double asterisk, respectively.

Datasets	Trend (K/8 years)	$StdDev_{Residuals}$(K)
	70° S to 70° N	
RAOBCORE-RO	+0.050 ± 0.064	0.10
RICH-RO	−0.041 ± 0.068	0.10
UAH-RO	−0.195 ± 0.036**	0.06
RSS-RO	−0.183 ± 0.039**	0.06
STAR-RO	−0.204 ± 0.037**	0.06
	20° S to 20° N	
RAOBCORE-RO	−0.108 ± 0.101**	0.16
RICH-RO	−0.246 ± 0.101**	0.15
UAH-RO	−0.202 ± 0.047**	0.07
RSS-RO	−0.177 ± 0.058**	0.09
STAR-RO	−0.216 ± 0.051**	0.08
	30° N to 70° N	
RAOBCORE-RO	+0.049 ± 0.074	0.11
RICH-RO	−0.036 ± 0.070	0.11
UAH-RO	−0.214 ± 0.065**	0.10
RSS-RO	−0.185 ± 0.065**	0.10
STAR-RO	−0.219 ± 0.060**	0.09
	70° S to 30° S	
RAOBCORE-RO	−0.088 ± 0.139	0.21
RICH-RO	−0.137 ± 0.133**	0.20
UAH-RO	−0.195 ± 0.067**	0.10
RSS-RO	−0.218 ± 0.066**	0.10
STAR-RO	−0.190 ± 0.066**	0.10

AMTD
4, 2127–2159, 2011

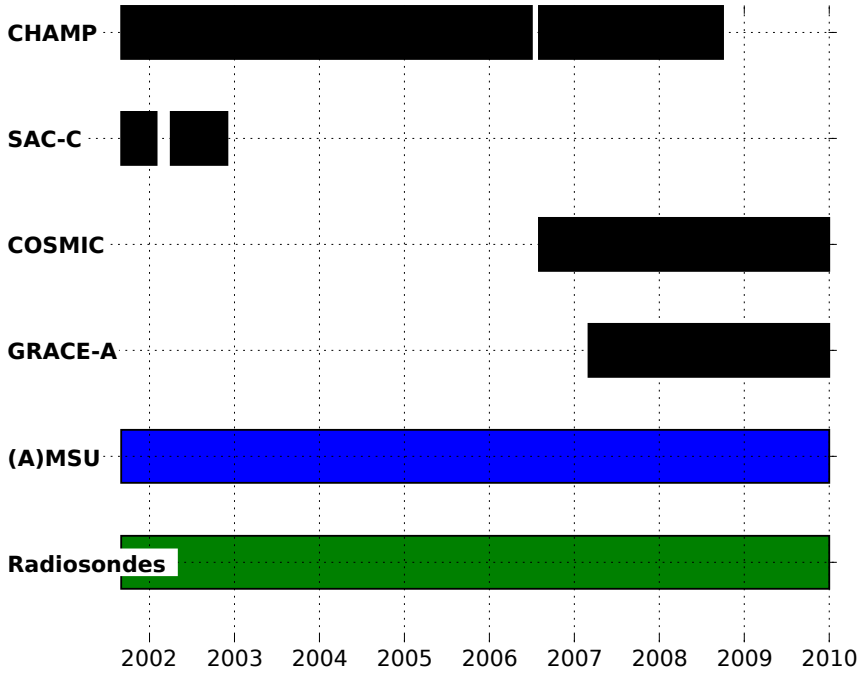

Fig. 1. Time frames of datasets used (black, GPS RO datasets).

AMTD
4, 2127–2159, 2011

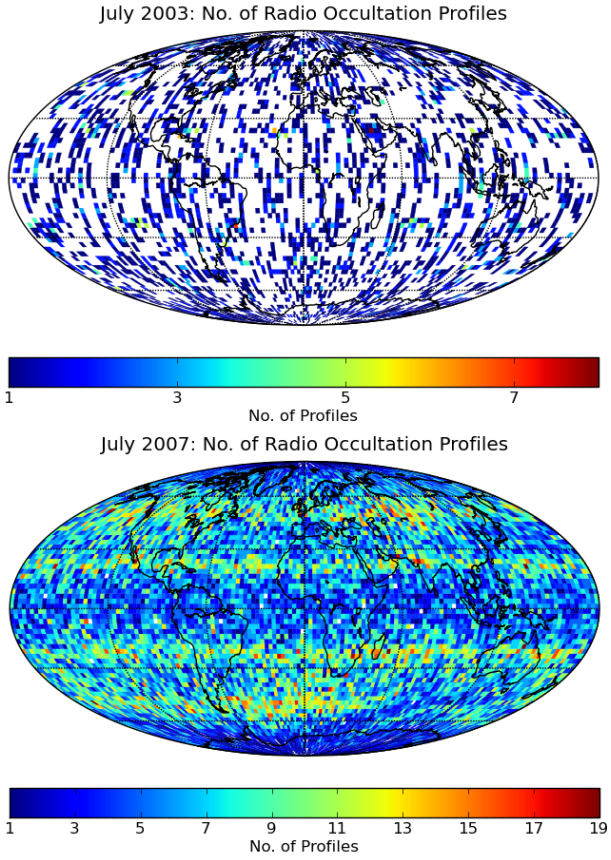

Fig. 2. Global monthly coverage of RO profiles for July 2003 (top) single-satellite (CHAMP) and for July 2007 (bottom) multi-satellite data (CHAMP, COSMIC, GRACE-A). Number of profiles in $2.5^{\circ} \times 2.5^{\circ}$ bins are shown.

AMTD
4, 2127–2159, 2011

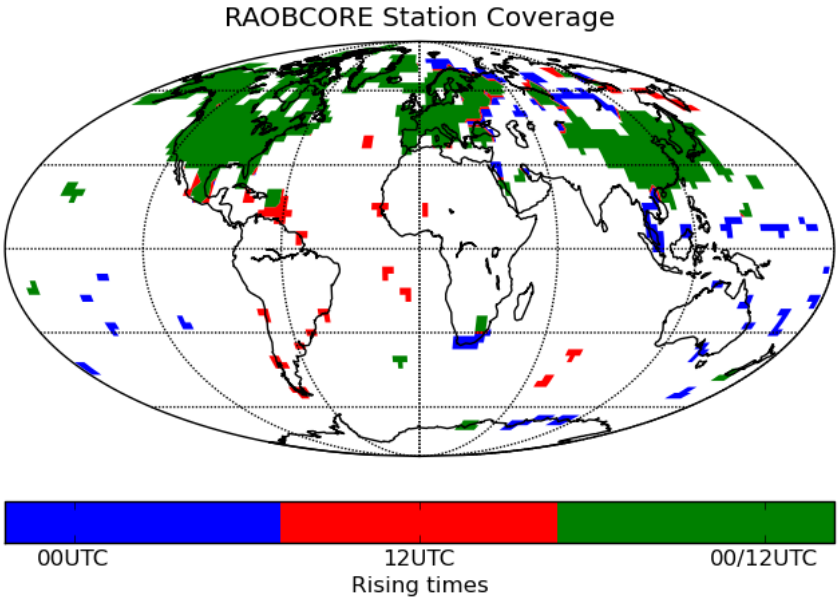

Fig. 3. Global coverage of radiosonde launches used in the RAOBCORE and RICH datasets. The color code shows whether there are launches at 00:00 UTC (blue), 12:00 UTC (red), or at both times (green), in the corresponding $2.5^{\circ} \times 2.5^{\circ}$ bin.

AMTD
4, 2127–2159, 2011

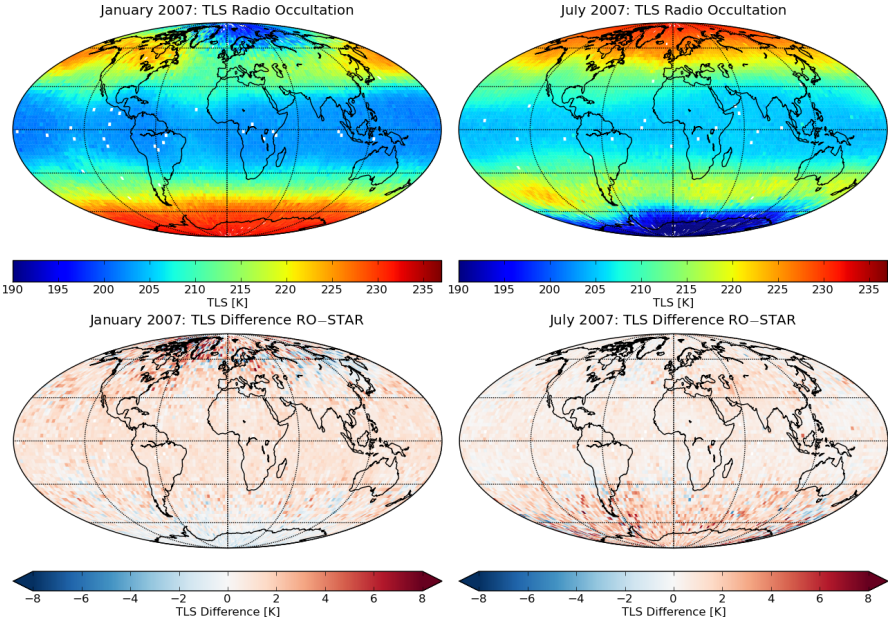

Fig. 4. Brightness temperatures (TLS) for two monthly means in 2.5° × 2.5° resolution. (left) January 2007, (right) July 2007, (top) Radio occultation synthetic TLS, (bottom) Difference of RO synthetic TLS to AMSU TLS (STAR).

AMTD
4, 2127–2159, 2011

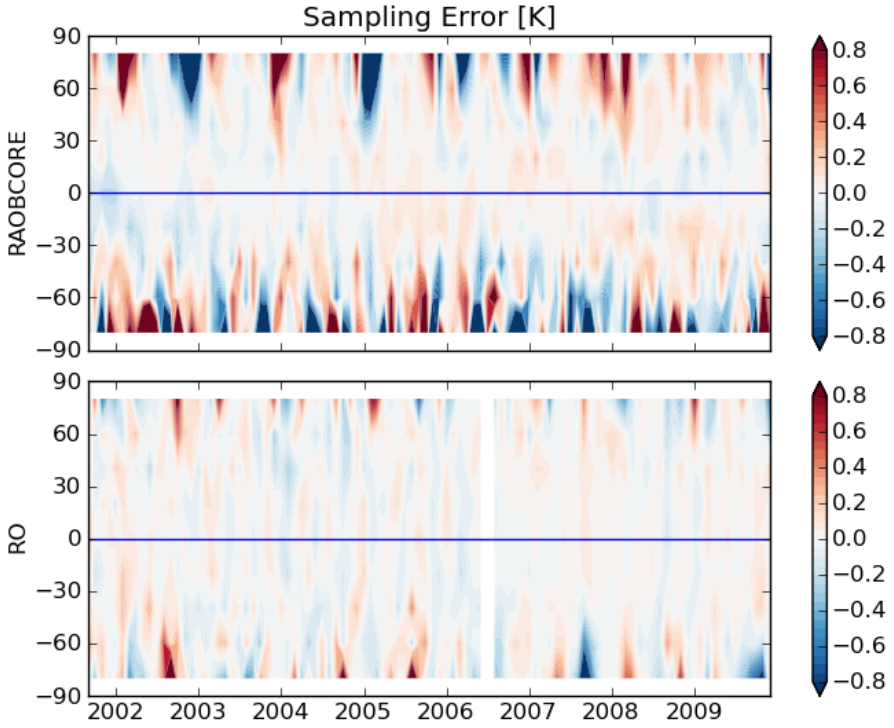

Fig. 5. Sampling error of (top) radiosondes and (bottom) RO. Shown are latitudinal bands in 20° resolution.

AMTD
4, 2127–2159, 2011

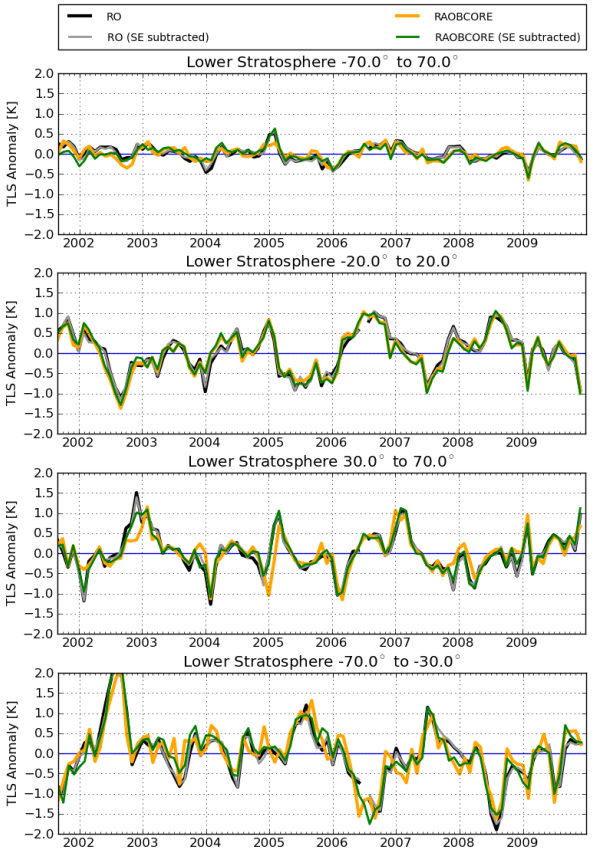

Fig. 6. TLS anomalies before/after subtracting the sampling error for RO (black/grey) and for RAOBCORE (orange/green). Shown for quasi-global region, tropics, and for NH/SH extratropics (top to bottom).

AMTD
4, 2127–2159, 2011

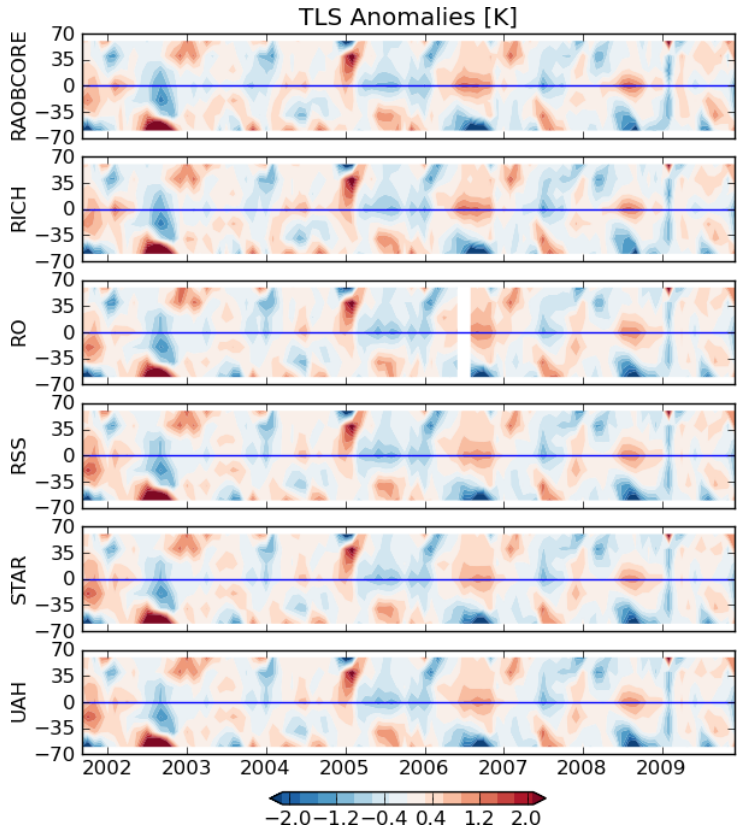

Fig. 7. Evolution of TLS anomalies for radiosondes (RAOBCORE, RICH), RO, and (A)MSU (RSS, STAR, UAH) (top to bottom), shown in 20° resolution.

AMTD
4, 2127–2159, 2011

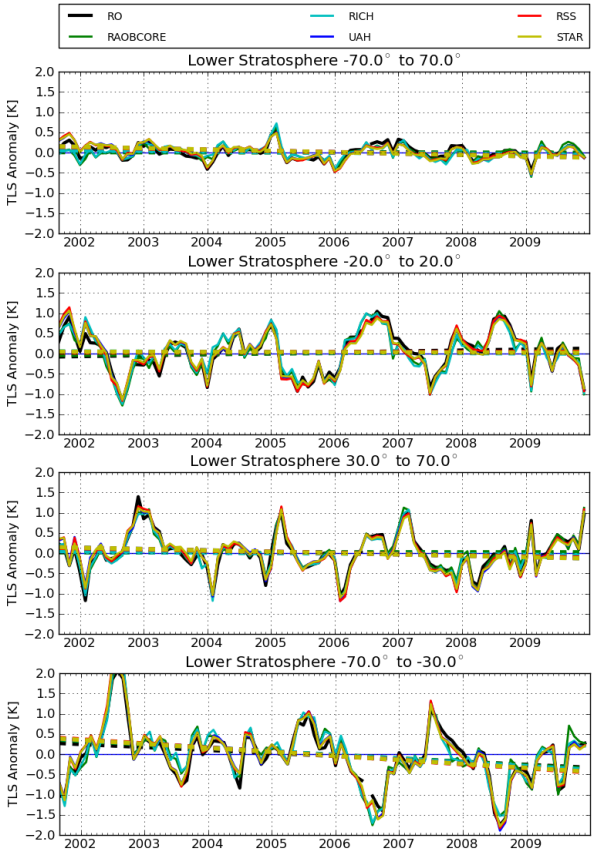

Fig. 8. TLS anomaly time series for all datasets, shown for quasi-global, tropical, and NH/SH extratropical zonal bands (top to bottom). The linear regression lines are shown as dashed lines.

AMTD
4, 2127–2159, 2011

Temperature record differences (A)MSU, radiosondes, GPS-RO

F. Ladstädter et al.

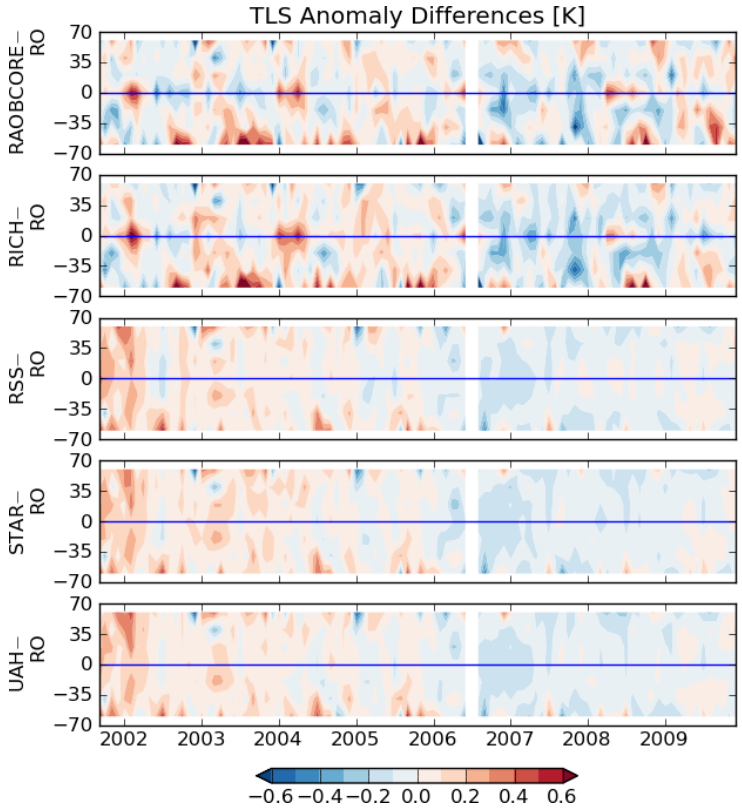

Fig. 9. Evolution of TLS anomaly differences of radiosonde (RAOBCORE, RICH) and (A)MSU (RSS, STAR, UAH) datasets to RO at 20° resolution (top to bottom).

AMTD
4, 2127–2159, 2011

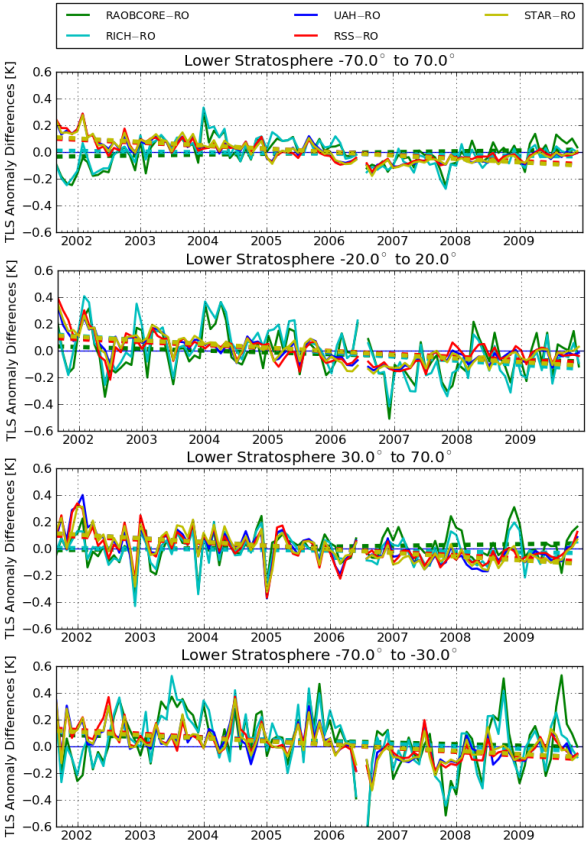

Fig. 10. TLS anomaly difference time series for all datasets, shown for quasi-global, tropical, and NH/SH extratropical zonal bands (top to bottom). The linear regression lines are shown as dashed lines.

AMTD
4, 2127–2159, 2011

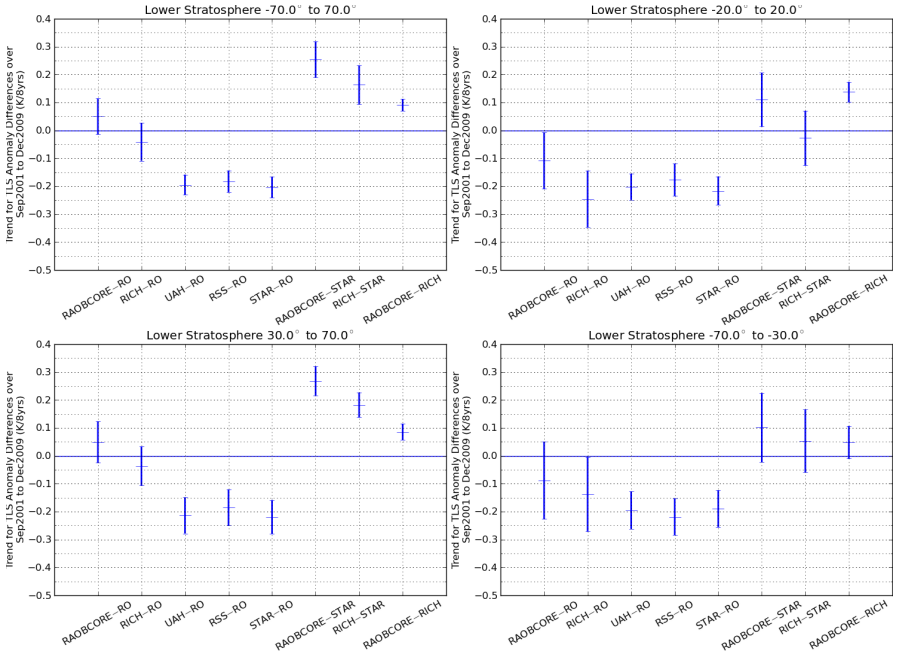

Fig. 11. Trend values of anomaly differences with 95% confidence interval for quasi-global, tropics, and NH/SH extratropics regions (top left to bottom right).

AMTD
4, 2127–2159, 2011